




# An investigation of the fluid-holding cavities in a lignocellulose-based bamboo matrix via a combined X-ray microtomography and proton time-domain NMR approach

Elton Jorge da Rocha Rodrigues · Roberto Pinto Cucinelli Neto ·  
Haimon Diniz Lopes Alves · Sidnei Paciornik · Druval Santos de Sá ·  
Khosrow Ghavami · Omar Ginoble Pandoli 

Received: 2 January 2023 / Accepted: 7 April 2023 / Published online: 18 April 2023  
© The Author(s) 2023

**Abstract** Bamboo (*Dendrocalamus giganteus*) is a functionally graded material with well-organized hierarchical structures. Its micrometer-sized vascular bundles and parenchymatic living cells allow an efficient upward flow of water and nutrients, endowing the organism with remarkably fast growth. As demonstrated recently, the hollow microstructure channels can be explored as a natural template for microfluidics applications in chemical synthesis, analytical detection, solar steam generation, and electrochemical devices. Thus, the knowledge of the kinetics of the imbibition and spatial distribution of fluid through the microcavities of the bamboo vegetal tissue became of interest. Here, we employed a combination of X-ray microtomography ( $\mu$ CT) and proton time-domain NMR (TD-NMR) to identify, measure, and investigate empty volumes embedded in the bamboo's tissue

as experienced by different organic and inorganic fluids, namely dimethyl sulfoxide (DMSO) and distilled water ( $H_2O$ ). Results have shown that the extensive communication between the voids (parenchymal cells and vascular channels) does not prevent the individuation of fluid reservoirs with different behaviors, as evidenced by the  $H_2O$  desorption profile. Bamboo parenchyma was the tissue that retained more residual  $H_2O$  after desorption. The difference in wettability of bamboo tissues by DMSO and  $H_2O$  was detected.

E. J. da Rocha Rodrigues · R. Pinto Cucinelli Neto  
Laboratório de Serviços em Relaxometria, Instituto de Macromoléculas Professora Eloisa Mano, Universidade Federal do Rio de Janeiro, Av. Horácio Macedo, 2.030, Rio de Janeiro 21941-598, Brazil

H. Diniz Lopes Alves  
Departamento de Física Aplicada e Termodinâmica, Instituto de Física, Universidade Estadual do Rio de Janeiro, Rua São Francisco Xavier, 524, Bloco B, Rio de Janeiro 20550-900, Brazil

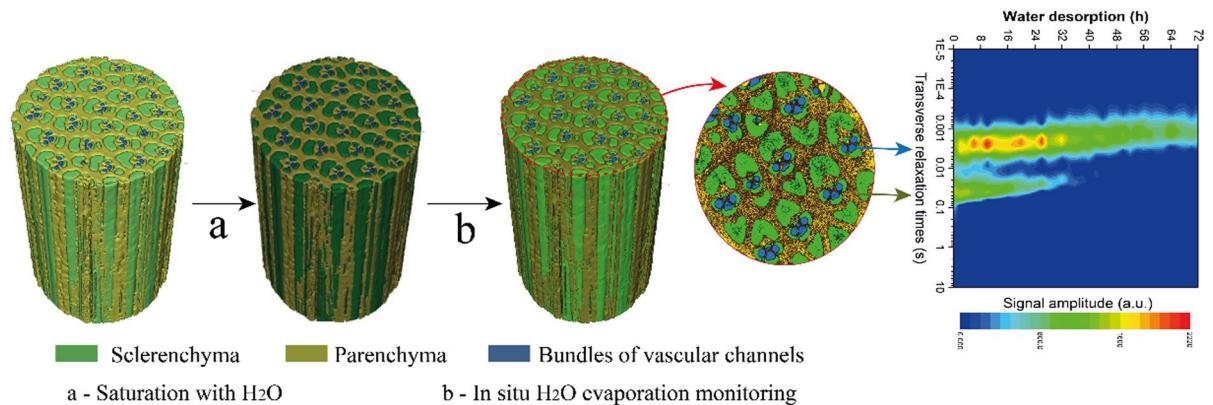
S. Paciornik  
Departamento de Engenharia Química e Materiais, Pontifícia Universidade Católica, Rua Marquês de São Vicente, 225, Rio de Janeiro 22451-900, Brazil

D. Santos de Sá · O. Ginoble Pandoli (✉)  
Departamento de Química, Pontifícia Universidade Católica, Rua Marquês de São Vicente, 225, Rio de Janeiro 22451-900, Brazil  
e-mail: omarpandoli@puc-rio.br; omar.ginoblepandoli@unige.it

K. Ghavami  
Departamento de Engenharia Civil, Pontifícia Universidade Católica, Rua Marquês de São Vicente, 225, Rio de Janeiro 22451-900, Brazil

*Present Address:*  
O. Ginoble Pandoli  
Dipartimento di Farmacia, Università degli Studi di Genova, Viale Cembrano, 4, 16148 Genoa, Italy

## Graphical abstract



**Keywords** TD-NMR · Real-time monitoring · X-ray microtomography · Surface relaxation · Bamboo · Lignocellulosic polymer

## Introduction

The bamboo (*Dendrocalamus giganteus*) plant tissue matrix is chemically and morphologically complex. It is considered an intelligent functionally graded material with oriented, hierarchical, and shaped biological tissues that developed over long-term evolution and selection (Nogata and Takahashi 1995). At the molecular level, it consists mainly of cellulose, a linear polysaccharide, highly organized due to hydrogen bonds between the abundant hydroxyl moieties of  $\beta$ -(1-4)-D-glucopyranose monomers; hemicellulose, a branched polysaccharide of low crystallinity consisting of monosaccharide units of 5 to 6 carbons (mainly glucose, xylose, galactose, and mannose) and lignin, a heterogeneous phenolic macromolecule (Youssefian and Rahbar 2015). Both cellulose and lignin are responsible for the high mechanical properties displayed by the plant and are found in large quantities (55% and 25%, respectively) in the bamboo matrix (Ji et al. 2013; Youssefian and Rahbar 2015).

At the micrometric level, the bamboo tissues concentrate cavities where liquids can flow and be stored, being greatly responsible for its fast growth. In the longitudinal direction of the bamboo's culm, straight and parallel channels with diameters varying from a few tens to a few hundred micrometers compose the

phloem, protoxylem, and metaxylem vascular systems. These vascular bundles are mechanically protected by the sclerenchymatous tissue, mainly constituted of highly oriented, crystalline, and hierarchical ligno-carbohydrate complex (LCC) (Hao et al. 2018). Also present in the culm, polyhedral-shaped micro-metric cells, with highly lignified walls interconnected via micro- and nanostructures called pits, constitute the parenchyma tissue (Xu et al. 2011; Ji et al. 2013; Peng et al. 2013; Youssefian and Rahbar 2015; Ginoble Pandoli et al. 2019).

Functional gradients, heterogeneities, and highly anisotropic morphology of biological materials have recently attracted much attention in investigations concerning novel sustainable and high-performance materials (Liu et al. 2017). Bamboo, less than wood, has been explored for new challenging applications, adding mechanical (Jin et al. 2015a, b; Li et al. 2017a), optical (Wang et al. 2022), biological (Pandoli et al. 2016) and chemical properties (Palma et al. 2020; De Sá et al. 2022). In the literature reports concerning bamboo specimens, most chemical modifications were conducted on the external surface of the material. However, few reports have been published exploring the internal structure of bamboo as biotemplates for microfluidic chemical platforms (Kuan et al. 2015; De Sa et al. 2019; Li et al. 2022), steam generation (Sheng et al. 2020; Chen et al. 2021), and electrochemical devices (Pandoli et al. 2020). These works addressed different ways of taking advantage of the internal structure of bamboo tissues, describing the filling and chemical functionalization of the

parenchyma and/or vascular bundles with transition metal salts or nanoparticles, such as copper and silver (Ginoble Pandoli et al. 2022, 2023). Recently, the anisotropic behavior of water vapor sorption into the hierarchical structure of bamboo was demonstrated, revealing different sorption directions, longitudinal (L) and transversal (T), for a saturated salt solution and water vapor (Chen et al. 2021). Thus, the need for a deeper understanding of how vascular channels and cell tissues interact with different fluids mainly used in organic chemistry has become evident.

X-ray microtomography ( $\mu$ CT) is a non-destructive technique widely used for the characterization of the microstructure of plants and has been used for bamboo as well (Palombini et al. 2020). Time-domain nuclear magnetic resonance (TD-NMR) is an efficient, fast, and non-destructive way to probe fluid behavior in confined environments (Steele et al. 2016; Singer et al. 2018). It is widely used in the study of oil reservoir rock matrices (Muhammad et al. 2014; Plastino et al. 2017; Rudszuck et al. 2019), water trapped in hydrogels (Rodrigues et al. 2016, 2017; Ratzsch et al. 2017) and to study the molecular dynamics of liquids during the hardening of cementitious materials (Valckenborg et al. 2001; Jansen et al. 2018).

TD-NMR has seen some uses in the study of liquids confined in vegetal tissue, including quantification of oil in seeds (Prestes et al. 2007; Colnago et al. 2011, 2014; Li and Ma 2021; Stagno et al. 2022). Zhang et al. (2016) used TD-NMR methods to characterize hierarchical pore structures in cotton fibers by measuring the different relaxation behaviors of the liquids imbibed in the cellulose matrix. The use of single-sided TD-NMR equipment is a very practical approach to study liquids in plant tissues (Menegazzo et al. 2020, 2021). Mohebbi et al. (2019) used the technique to quantify the amount of water in open foams and fibrous materials like paper. Li et al. (2017b) determined the rate of humidity desorption in wood (*Populus platyphylla* and *Pinus sylvestris*) samples via TD-NMR. Mikac et al. (2021) used magnetic resonance imaging (MRI) and TD-NMR methods to investigate the behavior of moisture content in *Fagus sylvatica* branches. Water uptake and moisture content in plant tissues were also investigated by Gezici-Koç et al. (2017) and Longo et al. (2023). Recently, Li and Ma (2022) proposed the investigation of the cell wall water of wood in the hygroscopic range using 2D TD-NMR, successfully differentiating

the water mobility in cellulosic material. Some other examples of 2D TD-NMR experiments applied to the investigation of water molecules behavior in wood samples were reported by Cox et al. (2010), Bonnet et al. (2017) and Stagno et al. (2021).

The interest in investigating the behavior of fluids in the cavities of harvested and treated bamboo emerges when its use as a renewable platform for carrying out physicochemical processes becomes evident. However, morphological heterogeneities in the cavities that retain and transport fluids inside the living plant can be found in each internode. Therefore, the structure-properties relationship in this context is highly relevant for the current and future applications of this class of renewable porous material.

In this work, we analyzed the behavior of organic (dimethyl sulfoxide) and inorganic (distilled water) fluids in the lignocellulosic matrix of bamboo (*D. giganteus*) through proton TD-NMR experiments, with the support of qualitative and quantitative structural data extracted from  $\mu$ CT analysis.

## Experimental

### Bamboo sampling

Bamboo specimens consisted of cylinders of 1 cm in height and 0.6 cm in diameter, extracted from internode number 3 closer to the ground. The sampling process is illustrated in Fig. 1. Considering the radial direction from the outer to the inner wall of the internode, we cut specimens at the external (close to the bark), intermediate and internal parts. The bamboo samples will be referred to as External for the outermost fraction, Middle for the intermediate fraction, and Internal for the innermost fraction. To eliminate organic residues, samples were washed under magnetic stirring in distilled water at 60 °C for 2 h. The samples were dried in an oven at 100 °C until constant mass.

### Probe fluids

Initially, we selected a wide range of organic and inorganic fluids to serve as a relaxation probe in the experiments. However, due to issues such as high volatility (methanol, ethanol, chloroform, tetrahydrofuran), which could prevent some of the lengthier

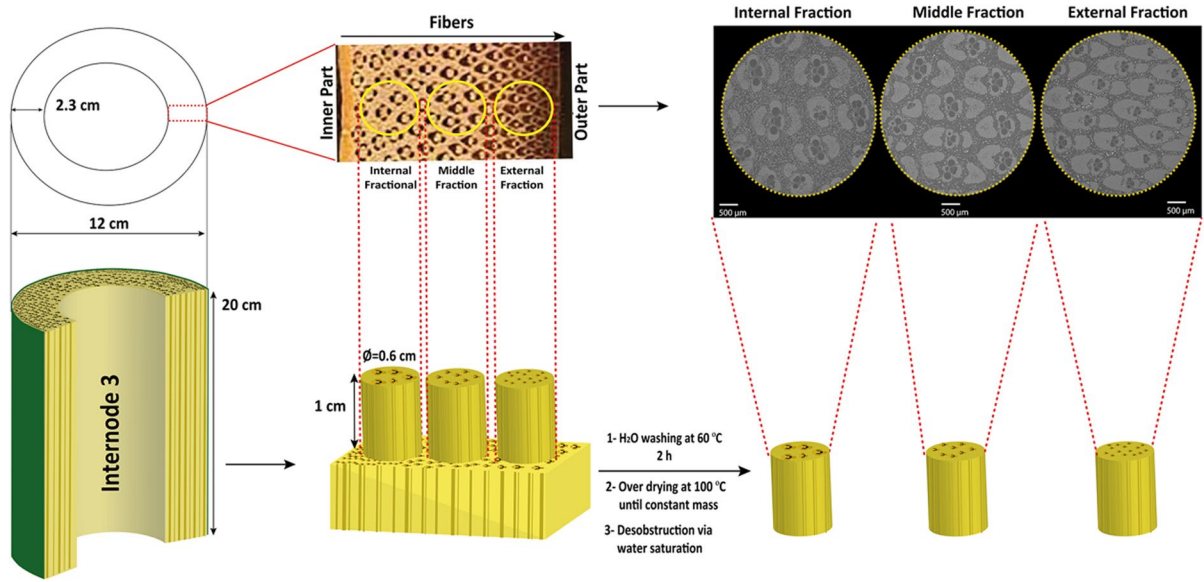
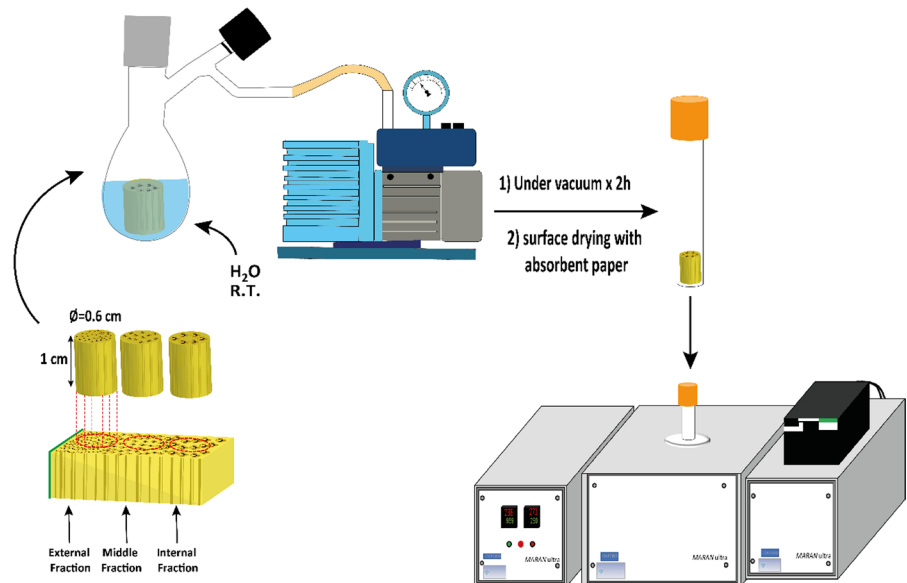


**Fig. 1** Bamboo sampling, conditioning, washing, and drying steps

**Fig. 2** Distilled water saturation of the bamboo fractions for TD-NMR analysis



experiments, we finally chose two solvents with high boiling points. Distilled water (H<sub>2</sub>O) (resistivity of 18 MΩ, filtered through a 0.22 μm mesh membrane, Milli-Q Gradient System A10, Millipore, USA) and dimethyl sulfoxide (DMSO) (ACS Reagent, Sigma-Aldrich, St. Louis, USA) were selected due to their low volatility, varying polarity values and different capacity for establishing physicochemical interactions with the lignocellulosic matrix of the bamboo plant.

#### Probe fluids saturation of the bamboo sample fractions

We conducted the saturation of the bamboo samples (external, middle, and internal) with each probe fluid using a vacuum chamber (Fig. 2). First, the samples were oven-dried at 100 °C until constant mass. Then, they were submerged in a given fluid volume (usually 5 mL of DMSO or H<sub>2</sub>O) inside

a Schlenk flask connected to a vacuum line. At this point, the samples remained afloat in the liquid. The system remained under reduced pressure (760 mmHg) for 2 h. When the vacuum was broken, the samples sank into the fluid, suggesting extensive filling of their structural cavities. To avoid interfering with the water content inside the bamboo sample's tissues we only surface-dried them with absorbent paper, weighed them again, and taken to the proton time-domain nuclear magnetic resonance equipment for analysis. The samples were taken to an oven at 100 °C for drying to constant mass before changing the type of probe fluid. All gravimetric measurements were conducted with a precision scale, with a resolution of 0.0001 g. All weighings were conducted in triplicate and reported as a mean with standard deviation values.

#### X-ray microtomography ( $\mu$ CT)

The 3D images of dry bamboo samples were obtained using a Zeiss Xradia 510 Versa microtomograph to visualize and quantify the 3D structure. The experimental parameters for all samples can be found in Table 1.

The images were processed using the CTan software (version 1.18.8.0, Bruker, 2018) and Avizo© software (version 9.0.1, FEI, 2018). Image pre-processing using a non-local means filter was used to improve the signal-to-noise ratio. Smaller regions of interest were delimited around the sample's image to remove the background and reduce computational requirements. Watershed segmentation (ThermoFisher Scientific 2018) as used to automatically separate the structures of interest (sclerenchyma, parenchyma, and vascular channels). Segmented images with each structure, i.e., parenchyma and vascular channels were then used for quantification.

**Table 1** X-ray microtomography ( $\mu$ CT) experimental parameters

Objective lens	4X
Pixel size ( $\mu$ m)	4.49
Voltage (kV)	50
Power (W)	4
Exposure time (s)	1.5
Number of projections	1601

The entire volume was measured, and the mean diameter was calculated for the whole 2D sections of the samples.

#### $^1\text{H}$ time-domain nuclear magnetic resonance (TD-NMR)

All measurements were performed on a MARAN Ultra (Oxford Instruments®) low-resolution NMR spectrometer operating at 0.54 T (23 MHz,  $^1\text{H}$  Larmor frequency) equipped with an 18 mm diameter probe at  $30 \pm 1$  °C. The  $90^\circ$  (p90) RF pulse was calibrated to 7.5  $\mu$ s, and the  $180^\circ$  (p180) pulse was calibrated to 15  $\mu$ s. Coil dead time and filter stabilization time were set to 6.0 and 3.0  $\mu$ s, respectively.

We employed the CPMG (Carr-Purcell-Meiboom-Gill) pulse sequence with 2048 points, with a time between echoes ( $2\tau$ ) of 600  $\mu$ s. For each sample, 64 scans were accumulated, with a recycle delay of 5 s. Total acquisition time was around 7 min. We carefully chose this interval between echoes to exclude the bulk of the relaxation signal from the lignocellulosic matrix's protons.

For measurements of the fluids' molecular dynamics in non-dynamic conditions, the samples saturated with each fluid were inserted in the TD-NMR tubes, and CPMG curves were acquired and stored for later processing. For the fluid desorption experiment, a given sample was filled with  $\text{H}_2\text{O}$  with the aid of the vacuum chamber, then superficially dried with a paper towel, and then left inside an open TD-NMR tube at 30 °C. The equipment was then set to acquire and store a CPMG curve immediately after the sample insertion and then at 2 h intervals for five days (120 h).

#### TD-NMR data processing

Data processing was conducted with the aid of commercial software. For the Inverse Laplace Transform (ILT), we employed WinDXP® Toolbox 1.8.1.0 (Resonance Instruments®), with a smoothing parameter set at  $2 \times 10^{-4}$  and tolerance at  $10^{-7}$ . A maximum of 50 iterations was allowed. None of the 2048 points obtained from the CPMG relaxation curve was excluded during the ILT processing, and all distribution curves were constructed with 256 points between



10  $\mu\text{s}$  and 10 s. All curve fitting procedures were made in Origin 8.5 (OriginLab®).

The Solid-Echo pulse sequence (SEPS) was used to evaluate the influence of the presence of the fluid inside the polymer matrix of the inner walls of the bamboo sample. The decay signal was acquired with 3072 points spaced by 1  $\mu\text{s}$ , with a receiver gain of 40 dB and a recycle delay of 2 s. The obtained FID signal was adjusted according to the following function:

$$A(t) = F_r \exp\left[\left(\frac{-t}{T_{2*}^R}\right)^2\right] + F_{sr} \exp\left[\left(\frac{-t}{T_{2*}^{SR}}\right)\right] + F_m \exp\left[\left(\frac{-t}{T_{2*}^M}\right)\right] + k \quad (1)$$

where,  $A(t)$  is the total amplitude of the FID signal,  $F_r$  is attributed to highly rigid molecular fractions and is written as a stretched exponential function to better fit the Gaussian contribution arising from residual dipolar coupling,  $F_{sr}$  is associated with molecular fractions with intermediate molecular mobility and  $F_m$  is the term related to highly mobile molecular fractions.  $T_{2*}$  refers to a transverse relaxation time, a constant related to the loss of phase coherence in the total magnetization of a given sample, provoked by inhomogeneities in the magnetic field and distinct physico-chemical environments in the sample. Finally,  $k$  is an offset parameter. Physical interpretations of the fractions and their respective relaxation times are given in the discussion section.

From the decomposition of the signal into the respective components, the average residual dipole coupling  $\langle M_2 \rangle$  was extracted from the adjustment of the component Fr with the function below:

$$G(t) = \exp\left(-\frac{1}{2M_2 t^2}\right) \quad (2)$$

Furthermore, the theoretical background for attributions of the behavior of liquid molecules in confined spaces such as pores, voids, and channels is given below. The ILT can be applied to the NMR decay signal to detect and discriminate the relaxation behavior of water protons in different families of pore sizes. The transverse relaxation rate of a liquid within porous materials is governed by the rates of free solvent relaxation ( $T_{2F}$ ), surface relaxation ( $T_{2S}$ ),

and diffusion resulting from molecular diffusion ( $T_{2D}$ ) (Zhang et al. 2016):

$$\frac{1}{T_2} = \frac{1}{T_{2F}} + \frac{1}{T_{2S}} + \frac{1}{T_{2D}} \quad (3)$$

$1/T_{2D}$  is the relaxation time caused by the diffusion of solvent molecules in the presence of internal field gradients being equal to  $(\tau\gamma G)^2 D/3$ . The time between echoes is  $\tau$ ,  $\gamma$  is the gyromagnetic ratio,  $G$  is the field-strength gradient and  $D$  is the molecular diffusion coefficient. The internal gradient is dependent on the strength of the applied magnetic field. For PSD analysis where the time between echoes is short enough (2 ms or smaller) in low-field spectrometers, this term of the equation also becomes greatly reduced, allowing the simplification of the equation. Thus, considering that  $T_{2F} \gg T_{2S}$  and a system within a fast diffusion limit, the equation can be approximated to (Al-Mahrooqi et al. 2006; Capitani et al. 2012; Meyer et al. 2018; Stagno and Capuani 2022):

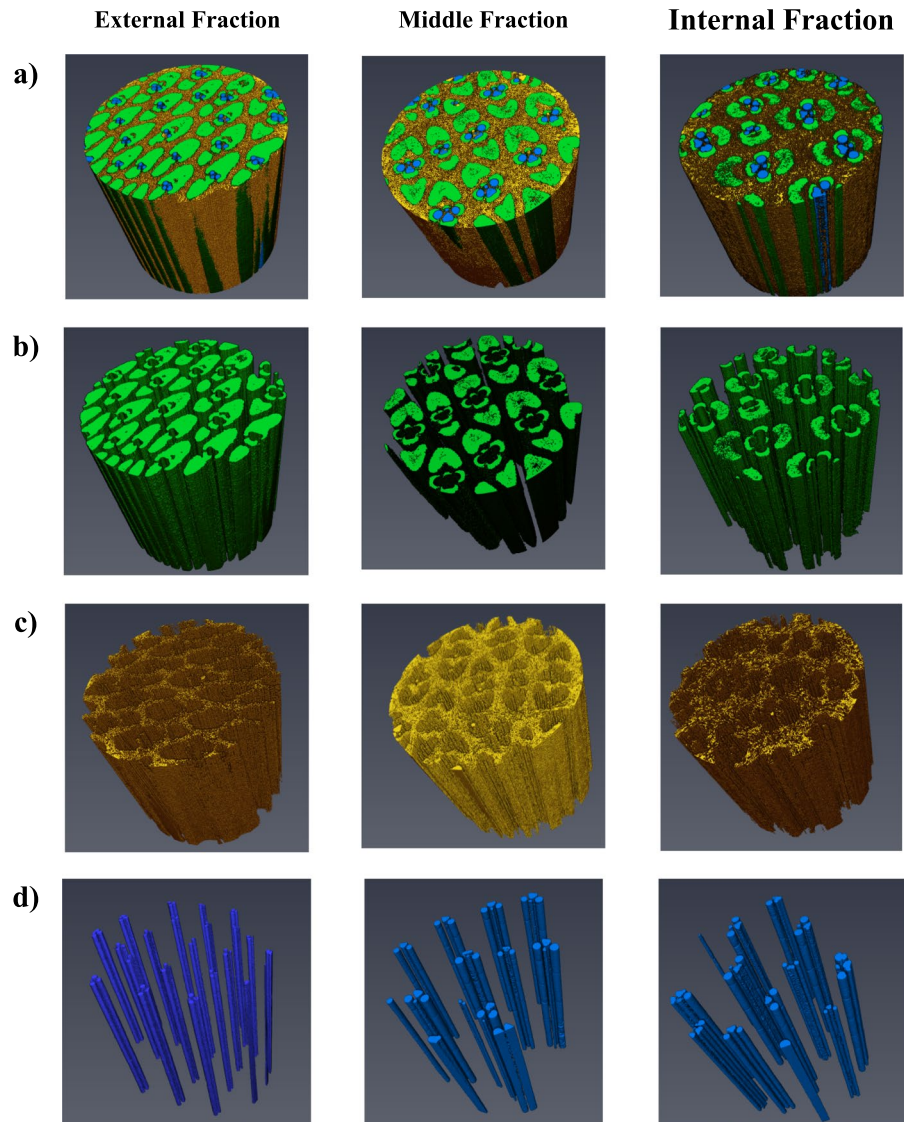
$$\frac{1}{T_2} = \frac{1}{T_{2S}} = \rho \frac{S}{V} \quad (4)$$

where  $S$  is the pore surface area,  $V$  is the pore volume, and  $\rho$  is the relaxivity constant of the confined fluid. For a given  $\rho$ , as  $\frac{S}{V}$  is proportional to  $\frac{1}{R}$  for a sphere, one sees that the transverse relaxation rate is directly proportional to the pore size (Zhang et al. 2016).

The surface contour maps used to report the behavior of the transversal relaxation domain curves of the water during its desorption at room temperature in the bamboo samples were generated by the Origin software. From the amplitudes of the 256 points generated by the ILT on the transverse relaxation data of the samples varying as a function of the desorption time, the software builds a matrix and assigns colors to the different values found in said matrix. Thus, it is possible to follow the evolution of the behavior expressed by the data over time and investigate dynamic processes in a visual and relatively simple way.

The values displayed in Table 4 were obtained using the value of the areas of the transverse relaxation curves generated by CPMG. For that, only the curves at the beginning of the desorption process were used (Time 0), corresponding to the maximum saturation value by fluids of those samples. Thus, for

**Fig. 3**  $\mu$ CT 3D images of the fractions sampled from the bamboo internode. In each group, the following structures are displayed: **a** the whole sample; **b** the sclerenchyma; **c** the parenchyma and; **d** the bundles of vascular channels



a given reservoir (free fluid, parenchyma, or vascular channels) the area under the corresponding curve was divided by the total area.

## Results and discussion

The highly anisotropic 3D architecture of the bamboo vegetal tissues was investigated by  $\mu$ CT, as shown in Fig. 3. The variation and spatial distribution of the different biological tissues were analyzed through segmentation and post-processing  $\mu$ CT images. Sclerenchyma tissue with its lignin-rich fibers (green, Fig. 3b) presents a variation in morphology and

density along the radial direction from the outer to the inner wall. Accordingly, the diameters of longitudinally-oriented vascular channels (blue, Fig. 3d) imbibed in the sclerenchyma tissue varied from  $121 \pm 27$  to  $192 \pm 32$   $\mu\text{m}$ . Here it is helpful to note that we call the plant's phloem, xylem, and metaxylem channels collectively “vascular bundle” and “vascular channels.” The parenchyma (yellow, Fig. 3c) is distributed throughout the volume of the sample. The volume occupied by parenchyma tissue cells and vascular channels in bamboo samples from each fraction is described in Table 2. Together, the vascular channels and the living cells of the parenchyma represent

**Table 2** Volumes occupied by the microcavities in each fraction of the bamboo sample and diameter of the structures with voids in the plant tissues as obtained via  $\mu$ CT images

Sample fraction	Vascular channels volume ( $\text{mm}^3$ )	Parenchyma cortex volume ( $\text{mm}^3$ )	Vascular bundle diameter ( $\mu\text{m}$ )	Parenchyma cells diameter ( $\mu\text{m}$ )
Internal	3.25	14.14	$192 \pm 32$	$38 \pm 10$
Middle	3.01	11.76	$175 \pm 39$	$33 \pm 7$
External	2.20	8.03	$121 \pm 27$	$26 \pm 5$

**Table 3** Fluid's total mass in saturated bamboo samples

Sample fraction	$\text{H}_2\text{O}$ mass (g)*	DMSO mass (g)*
Internal	$0.1412 \pm 1.5 \times 10^{-4}$	$0.1024 \pm 1.1 \times 10^{-4}$
Middle	$0.1169 \pm 1.1 \times 10^{-4}$	$0.0867 \pm 5.7 \times 10^{-5}$
External	$0.0686 \pm 5.8 \times 10^{-5}$	$0.0502 \pm 5.8 \times 10^{-5}$

\*Masses are reported as the mean of triplicates with standard deviations

microcavities of different sizes and morphologies and are the focus of the present work. These structures play fundamental roles in the growth, mechanical strength, transportation, and storage of organic and inorganic materials needed to maintain vegetal homeostasis.

The cells of the parenchyma cortex and the fibrous bundles of the sclerenchyma, where the vascular channels are found, increase in size from the external to the internal fraction. This change directly affects the total fluid's mass that a given fraction of comparable dimensions can hold when fully saturated, as described in Table 3.

The discrepancy found in the masses of  $\text{H}_2\text{O}$  and DMSO in the saturated samples can be attributed to the different wettability capacities of the molecular structure of bamboo tissues composed of cellulose, hemicellulose, and lignin. The filling fluids used in this study differ in molecular mass, polarity, and the number of hydrogen bonds they can establish, with  $\text{H}_2\text{O}$  having a greater physicochemical affinity for the bamboo plant structure (Reichardt and Welton 2010).

The observation of cross sections obtained from  $\mu$ CT images (Fig. 4) of the three fractions indicates distinct volumes occupied by the plant's structures. For instance, in the internal fraction, one can clearly see the predominance of the parenchyma tissues. In fact, the abundance of the parenchyma tissue cavities in the internal fraction becomes evident when we observe the darkening of the yellow color of the generated CT image, suggestive of a less dense region. Although it is true that density plays a role in the different shades and colors on the images, we cannot ascribe the differences observed only to density gradients. Some of the variations in the color have been affected by the image processing software, even though we were trying to keep the same

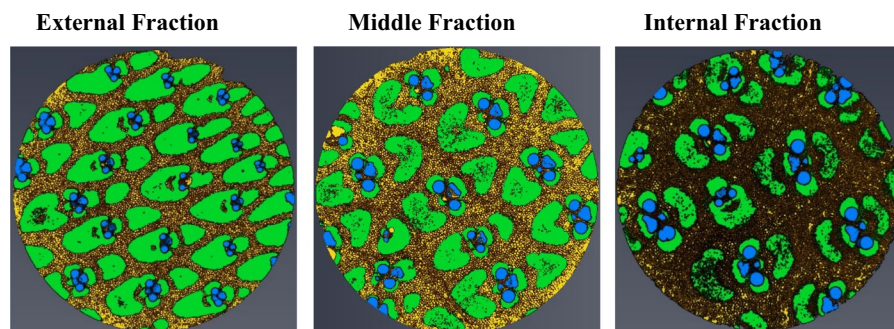


**Fig. 4**  $\mu$ CT images of the transverse section of each dry bamboo sample fraction. Several heterogeneities in the volume and spatial distribution of the fluid-holding compartments can be observed. The vascular channels are shown in blue,

and the parenchyma is shown in yellow. Furthermore, the fibrous shafts of the sclerenchyma (shown in green) display an increasing number of hollow sections from the External to the Internal fraction



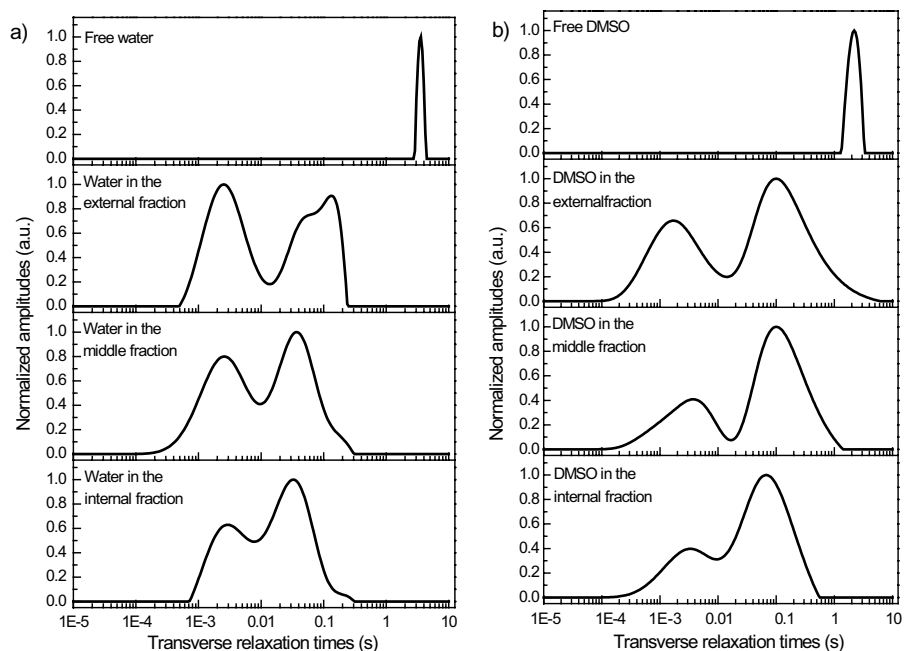
color palette for all images. The cell wall of the parenchyma cortex is populated by pit holes, cell-wall openings hundreds of nanometers in diameter, responsible for exchanging materials in the living plant. In the case of internal and middle fractions, the parenchyma cells present more surface area in contact with the vascular bundle channels offering extra possibilities of fluid exchange via pit holes (Pandoli et al. 2019). This can be seen in Fig. 4, where the channels (blue) are less embedded in the sclerenchyma tissues (green). In the external fraction, however, the architecture of the different tissues reduces the possibility of the facilitated fluid exchange found in the innermost fractions. In addition, the external fraction exhibits more massive fibrous bundles, unlike the innermost fractions of bamboo.

TD-NMR is very useful in probing the molecular mobility of a liquid phase embedded in a solid matrix (Meyer et al. 2018; Stagno and Capuani 2022). Through interferences in the relaxation processes, such as those described earlier, we can extract very accurate data about the environment in which the molecules in a liquid are confined. In Fig. 5a, b, we have the transverse relaxation time domain curves, obtained by the CPMG pulse sequence, of H<sub>2</sub>O and DMSO molecules in four different environments. The free water/DMSO curves

correspond to the behavior expected from a fluid when it is free from spatial confinement. That is, most of its molecules can undergo free rotation, and have higher mobility and free diffusion processes, implying bigger T<sub>2</sub> values (in the order of seconds). A fluid confined in a solid matrix suffers the effects of interaction between its molecules and the surrounding walls. In this scenario, surface relaxation, as described in Eq. 4, plays a relevant part and lowers the molecules mobility when compared to the bulk solvent (Zhang et al. 2016). Therefore, the smaller the pore size, the lower the molecular mobility of the solvent. (Al-Mahrooqi et al. 2006; Capitani et al. 2012). These effects interfere with the magnetic relaxation of the fluid molecules, widening the bases of the domain curves and significantly reducing the relaxation time values, as seen in Fig. 5.

The area under a relaxation domain curve can be related to the number of protons that relax in that time interval. We observed that the water molecules confined in bamboo cavities have at least two large relaxation domains: one at shorter times (tens of milliseconds) and the other at longer times (around 100 ms). Relaxation time values are inversely proportional to the confinement experienced by the fluid molecules (Zhang et al. 2016). Therefore, we can attribute the shortest relaxation times to the water molecules

**Fig. 5** Relaxation distribution curves, obtained via ILT on CPMG data, displaying the effect of physical confinement on water (a) and DMSO (b) molecules in four different environments



occupying the parenchyma cavities (left side) and the longest times to the water molecules occupying the vascular channels (right side). The same rationale can be applied to DMSO molecules.

There is a clear difference in the populations of fluid molecules in each of the bamboo fractions. In the internal fraction, the largest population is found inside the vascular channels; in the middle fraction, the population relative to the molecules of the fluid in the parenchyma starts to increase and, finally, in the external fraction, the amount of fluid contained in the parenchyma is slightly larger than that inside the vascular channels. Therefore, the importance of choosing which region of the plant becomes evident when technological applications of the material are envisioned. The results show that each fraction has a distinctive way of distributing fluid throughout its volume (Table 4).

From the distributions of transverse relaxation times, two relaxation domains are observed, both for the water-saturated bamboo and the DMSO-saturated bamboo. The domain with the lowest  $T_2$  value (approximately  $2 \times 10^{-3}$  s) is related to the solvent present in more confined spaces of the bamboo matrix, such as the parenchyma and sclerenchyma and the internal channels that connect the different regions of the bamboo. In addition, there is a fraction of the solvent on the surface of the inner walls of the vascular channels, where the effect of surface relaxation is more pronounced, which promotes the reduction of the  $T_2$  value compared to the free solvent (bulk) molecules.

The domain with the highest  $T_2$  value (approximately 0.1 s) is related to the solvent present in the vascular channels, more specifically in their central region, away from the internal walls. In this region's cross-section, the solvent molecules can be found in an unimpeded environment, translating to a relaxation regimen closer to their bulk state.

Similar trends are observed when we compare the internal, intermediate, and external bamboo fractions distribution for the water- and DMSO-logged samples. The domain with the lowest  $T_2$  value shifts to the shorter relaxation times for the outer fraction of the bamboo. However, the domain with the highest  $T_2$  value shifts to the right, increasing its value for the outermost fraction of the bamboo. The shortening of the relaxation times corroborates the data obtained from microtomography. As noted, parenchyma and

**Table 4** Distribution of H<sub>2</sub>O and DMSO molecules in each saturated bamboo fraction

Sample	Parenchyma cortex (%)		Vascular channels (%)	
	H <sub>2</sub> O	DMSO	H <sub>2</sub> O	DMSO
Internal fraction	36	27	64	73
Middle fraction	42	31	58	69
External fraction	52	38	48	62

sclerenchyma have the smallest pore sizes, which become even smaller as we advance from the inside to the outside of the bamboo. This higher confinement of the fluid translates into a reduction in the value of  $T_2$ .

The increase in the  $T_2$  value for the domain around 0.1 s can be explained by the more significant number of bundles of vascular channels present in the outermost fraction, as highlighted in Fig. 3. Although the diameters of the bundles are smaller in the outermost region of the bamboo, the channels have three-dimensional cylindrical structures, and each cylinder has a central region in which the fluids' molecules can relax their magnetization with less encumbrance; that is, they do not experience the effect of surface relaxation of the channel walls. Since the outermost fraction has more vascular channels, the amount of water in the bulk state is larger than in the innermost fraction of the bamboo. This, in turn, translates into an increase in the  $T_2$  value for the second domain shown in Fig. 5.

The difference in distribution profiles between water and DMSO should be highlighted. While the first solvent has narrower and more well-defined domains, the transverse relaxation distribution for DMSO shows a broader profile. From the presented data, we can infer that, while the bamboo tissues' water-saturation capabilities are extensive, as expected, the DMSO molecules can permeate with ease through the plant matrix. This information may be relevant when choosing the best solvent in a microfluidics process (Machado et al. 2014).

The Solid-echo pulse sequence (SEPS) was employed to investigate the effects of the saturation of water or DMSO (Fig. 6) molecules on the structure of the bamboo matrix. Solvents of different polarities act on the lignocellulosic chains. These observations

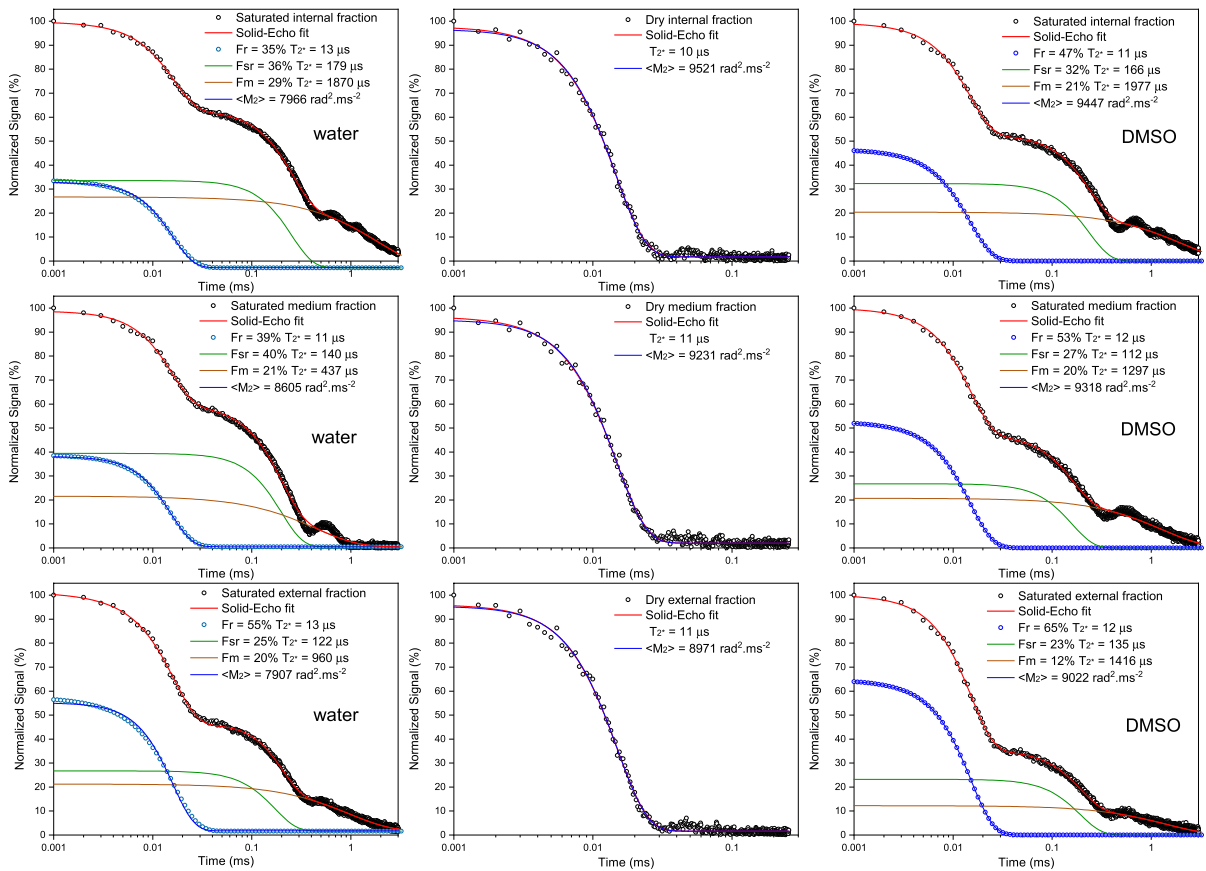


**Fig. 6** Obtained SEPS NMR signal intensities fitted to Eq. 1 (signal components) and Eq. 2 ( $M_2$  values) for the samples saturated with distilled  $H_2O$  (left) and DMSO (right). The middle column refers to the dry bamboo samples

seek the best performance of bamboo in microfluidics operations.

The FID measurements obtained by SEPS reveal three well-defined regions in the water-saturated (Fig. 6, on the left side) or DMSO-saturated bamboo structure (Fig. 6 on the right side). The rigid fraction ( $F_r$ ) is attributed to the sclerenchyma (crystalline cellulose), the semi-rigid fraction ( $F_{sr}$ ) is associated with the parenchyma, and the high mobility fraction ( $F_m$ ) refers to the inner walls of the vascular bundles. These vessels contain the solvent molecules relaxing closest to the bulk state, with high  $T_{2^*}$  values.

Relaxation signals for dry bamboo were obtained to evaluate the effect of the presence of water or DMSO on the three ( $F_r$ ,  $F_{sr}$ , and  $F_m$ ) relaxation regions of the bamboo. In the absence of solvent molecules, the bamboo polymeric matrix displays rigidity, as observed in the fast decay regimen of the NMR

signal (Fig. 6, middle column). The signal was fitted by a Gaussian function with a transverse relaxation time of about  $10 \mu s$  and a residual dipole coupling ( $M_2$ ) close to  $9000 \text{ rad}^2 \text{ ms}^{-2}$ . As expected, the presence of liquid molecules with chemical affinity with the natural polymer matrix increases the molecular mobility of the lignocellulosic structures constituting the samples, leading to the observed increase in the  $T_{2^*}$  values. Similar behavior was observed in the NMR relaxation of wood samples saturated with different fluids (Zhang et al. 2016).

For the samples saturated with water, a rising trend in the  $F_r$  contribution to the total magnetization in each sample is observed when we move from inner to outer fractions of the sample (35–55% of  $F_r$ ). As seen in the  $\mu CT$  results (Figs. 3, 4), the external fraction contains larger quantities of sclerenchyma, which displays very little permeability. The percentage of  $F_{sr}$

remains higher than  $F_m$  since the parenchyma volume is larger than the vascular bundles in the samples, as seen in Table 2.

Comparing the values of  $M_2$  for the dry ( $M_{2\text{average}} = 9241 \text{ rad}^2 \text{ ms}^{-2}$ ) and water-saturated bamboo samples ( $M_{2\text{average}} = 8159 \text{ rad}^2 \text{ ms}^{-2}$ ) for each of the sampling fractions, the internal fraction shows a reduction of 16% in this parameter, the highest variation in all three sampling fractions. This reduction reflects a small volume of sclerenchyma tissues (Table 4), implying a higher water-soaking ability. Furthermore, the analysis of the  $M_2$  values informs that solvation of the sclerenchyma with water and DMSO molecules has happened. We tentatively attribute this to the micro and nanometric pits interconnecting vascular bundles and sclerenchyma tissues, allowing for solvent flow between these regions.

The bamboo samples saturated with DMSO also display three well-defined regions, as described above. The  $F_r$  values (from 47 to 65%) are higher when compared to the results obtained with distilled water (from 35 to 55%). This feature, associated with the higher values of  $M_2$ , suggests that DMSO has lower permeability in the sclerenchyma than water. We attribute the rise in the  $F_r$  percentage from 47 (internal) to 65% (external) to the higher volume of sclerenchyma tissue in the external fraction.

Another important aspect is the  $T_{2*}$  values for the region of high mobility ( $F_m$ ) of the bamboo samples saturated with DMSO ( $T_{2*\text{average}} = 1563 \text{ ms}$ ), which are higher than those obtained with the water ( $T_{2*\text{average}} = 1089 \text{ ms}$ ). This suggests that DMSO molecules tend to occupy, preferably, the vascular bundle. Therefore, it is observed that ultrapure water, as expected, has a greater capacity to diffuse through the bamboo's internal structures, mainly due to polarity and molecular size and the ability to perform hydrogen bonds. Both solvents remain primarily in the parenchyma and vascular channels, but water also has a small capacity to permeate the sclerenchyma.

The evolution of the magnetic relaxation domain curves in TD-NMR as a function of time can be represented through contour surface maps (Rodrigues et al. 2018). The intensities and relaxation time values of the domains at each moment represent the dynamics of the water evaporating inside the bamboo cavities as a function of time. The water evaporation from bamboo samples was monitored in real-time by TD-NMR to describe the behavior and distribution of

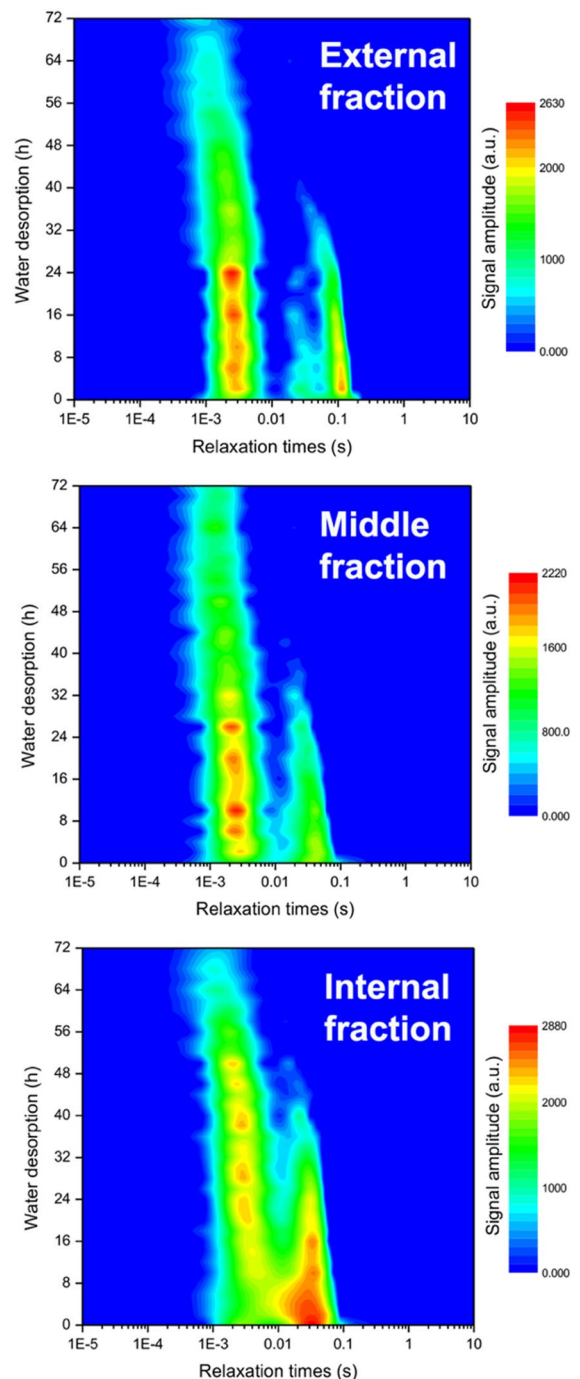


**Fig. 7** Surface contour plots of the 72 h long water desorption process are monitored in real time via the transverse relaxation of water molecules obtained via CPMG. The ILT curves are then plotted as function of desorption time



the water molecules inside the bamboo microcavities. Figure 7 shows the results obtained.

Initially, 120 h of process monitoring was recorded, but from 72 h onwards, the remaining amount of water becomes very small, and the signal-to-noise ratio greatly decreases. This compromises the quality of the Inverse Laplace Transform that generates the domain curves, which significantly reduces the reliability of the results.

A qualitative analysis of each contour surface map shows that the behavior of confined water during evaporation is different for each bamboo fraction. There are two large populations of water molecules represented by the two trails on the map: one at longer relaxation times relative to water in vascular channels and one at shorter relaxation times relative to the environment of the parenchyma cortex. The coalescence of the confined water molecules' transverse relaxation domains progressively increases from the outer to the inner fraction, again indicating the existence of varying degrees of connection between the two cavities in the tissue. We propose that this behavior becomes apparent in TD-NMR experiments from a certain threshold of water saturation, such as those used in this work.

Previous experiments with wood samples containing varying amounts of water did not report the present findings, as they operated inside a framework of water vapor saturation or natural humidity present in their samples (Mikac et al. 2021; Cousse et al. 2022; Li and Ma 2022). The extent of communication between the parenchyma cavities and the vascular channels became evident during the desorption experiment. The population of water molecules in vascular channels disappears after 48 h in the three fractions, albeit at different evaporation rates for each fraction. The water present in the smaller cavities of the parenchyma does not disappear completely, although the amplitude of these domains decreased considerably compared to the beginning of the evaporation process. It has been demonstrated that a residual amount of water is retained in lignocellulosic materials due to hydrogen interactions with the cellulose chains in plant tissue (Zhang et al. 2016; Li et al. 2017c).

Both the coalescence of the relaxation domains of water molecules and the time until the amplitude of these domains is considerably reduced by evaporation substantiate the results of  $\mu$ CT. Previous

studies have shown that the interconnected pore structure constitutes a highly specialized fluid transportation system (Liu et al. 2021). The efficiency of this system is evident when we examine the behavior of the confined water volume in the samples of the internal and middle fractions. In highly confined environments, the trapped water molecules have their evaporation rate delayed at temperatures close to room temperature, like those used in our experiments, which may explain the remaining amplitude of the observed relaxation domains even though it has long test times. We demonstrated that the efficiency of fluid exchange between the two types of microcavities (vascular bundles and parenchyma cells) becomes a relevant factor affecting the fluid's evaporation rate.

## Conclusions

$\mu$ CT and TD-NMR showed great potential for analysis of the internal structure of bamboo, as well as the distribution of solvents of different polarities and their effects on the molecular mobility of the fully solvent-saturated bamboo structure. The  $\mu$ CT results supported the reasoning used in the interpretation of the TD-NMR data. Most of the interpretations of the behavior of the molecular dynamics of the fluids confined in the bamboo structure were only possible with the aid of this technique's qualitative and quantitative information.

The CPMG sequence, through the values of  $T_2$  and the area under the distribution of domains, can map the distribution of solvents in the parenchyma and vascular channels, being sensitive to the morphology changes as a function of the bamboo cut region (internal, intermediate, or external), corroborating the data obtained by microtomography. Ultrapure water and DMSO showed similar distribution profiles. Monitoring water desorption indicates that it takes 40–48 h for almost all of the solvent to leave the bamboo matrix, leaving only a small fraction confined in the parenchyma.

The Solid Echo sequence, through the  $T_{2*}$  values and the percentages of rigid, semi-rigid, and mobile fractions, was sensitive to the mobility variations of the lignocellulosic chain segments in the presence of ultrapure water or DMSO. The results indicate that water has a greater permeation capacity and affects

the rigid fraction of bamboo more, while DMSO settles more easily in vascular channels.

We believe that the data found in this work may be fundamental in choosing the most suitable solvent for a particular type of bamboo during a microfluidic process, as well as its effects on the structure of the segments of the bamboo chain.

In general, the results indicate dependence between the physicochemical characteristics of the fluids and lignocellulose-based microfluidic reactors with hierarchical architecture, such as bamboo. Studies with other fluids and ionic liquids are being conducted by our group to understand better the molecular behavior in confined environments made up of natural polymers.

**Author contributions** Conceptualization: OGP, EJRR, data curation: OGP, EJRR, RPCN, HDLA, funding acquisition: OGP, SP, KG, investigation: OGP, EJRR, RPCN, HDLA, DSS, project administration: OGP, SP, KG, supervision: OGP, SP, KG, RPCN, validation: OGP, EJRR, RPCN, visualization: EJRR, RPCN, HDLA, DSS, writing original draft: OGP, EJRR, RPCN, DSS, writing-review and editing: OGP, EJRR, RPCN, DSS, SP, KG.

**Funding** Open access funding provided by Università degli Studi di Genova within the CRUI-CARE Agreement. The study was supported by the Serrapilheira Institute (Grant Number Serra-1709-17482), Conselho Nacional de Desenvolvimento Científico e Tecnológico-Brasil (CNPq) (458302/2013-9), Fundação Amparo à Pesquisa do Estado do Rio de Janeiro (FAPERJ) (E-26/010.100622/2018, E-26/010.001646/2019, SEI-260003/001227/2020, E-26/010.000980/2019 and E-26/202.409/2021) and Coordenação de Aperfeiçoamento de Pessoal de Nível Superior—Brasil (CAPES)—Finance Code 001.

**Data availability** All data generated or analyzed during this study are included in this published article.

## Declarations

**Conflict of interest** There are no conflicts of interest/competing interests.

**Ethical approval** No results of studies involving humans or animals are reported.

**Open Access** This article is licensed under a Creative Commons Attribution 4.0 International License, which permits use, sharing, adaptation, distribution and reproduction in any medium or format, as long as you give appropriate credit to the original author(s) and the source, provide a link to the Creative Commons licence, and indicate if changes were made. The images or other third party material in this article are included in the article's Creative Commons licence, unless indicated

otherwise in a credit line to the material. If material is not included in the article's Creative Commons licence and your intended use is not permitted by statutory regulation or exceeds the permitted use, you will need to obtain permission directly from the copyright holder. To view a copy of this licence, visit <http://creativecommons.org/licenses/by/4.0/>.

## References

- Al-Mahrooqi SH, Grattoni CA, Muggeridge AH et al (2006) Pore-scale modelling of NMR relaxation for the characterization of wettability. *J Pet Sci Eng* 52:172–186. <https://doi.org/10.1016/j.petrol.2006.03.008>
- Bonnet M, Courtier-Murias D, Faure P et al (2017) NMR determination of sorption isotherms in earlywood and latewood of Douglas fir. Identification of bound water components related to their local environment. *Holzforchung* 71:481–490. <https://doi.org/10.1515/hf-2016-0152>
- Capitani D, Di Tullio V, Proietti N (2012) Nuclear magnetic resonance to characterize and monitor cultural heritage. *Prog Nucl Magn Reson Spectrosc* 64:29–69. <https://doi.org/10.1016/j.pnmrs.2011.11.001>
- Chen Q, Fang C, Wang G et al (2021) Water vapor sorption behavior of bamboo pertaining to its hierarchical structure. *Sci Rep* 11:12714. <https://doi.org/10.1038/s41598-021-92103-4>
- Cocusse M, Rosales M, Maillet B et al (2022) Two-step diffusion in cellular hygroscopic (vascular plant-like) materials. *Sci Adv* 8:1–17. <https://doi.org/10.1126/sciadv.abm7830>
- Colnago LA, Azeredo RBV, Marchi Netto A et al (2011) Rapid analyses of oil and fat content in agri-food products using continuous wave free precession time domain NMR. *Magn Reson Chem* 49:S113–S120. <https://doi.org/10.1002/mrc.2841>
- Colnago LA, Andrade FD, Souza AA et al (2014) Why is inline NMR rarely used as industrial sensor? Challenges and opportunities. *Chem Eng Technol* 37:191–203. <https://doi.org/10.1002/ceat.201300380>
- Cox J, McDonald PJ, Gardiner BA (2010) A study of water exchange in wood by means of 2D NMR relaxation correlation and exchange. *Holzforchung*. <https://doi.org/10.1515/hf.2010.036>
- da Rodrigues EJR, de Cavalcante MP, Tavares MIB (2016) Time domain NMR evaluation of poly(vinyl alcohol) xerogels. *Polímeros* 26:221–227. <https://doi.org/10.1590/0104-1428.2093>
- da Rodrigues EJR, Neto RPC, Sebastião PJO, Tavares MIB (2018) Real-time monitoring by proton relaxometry of radical polymerization reactions of acrylamide in aqueous solution. *Polym Int* 67:675–683. <https://doi.org/10.1002/pi.5546>
- De Sa DS, Bustamante RDA, Eduardo C et al (2019) Fabrication of lignocellulose-based microreactors: copper-functionalized bamboo for continuous-flow CuAAC click reactions. *ACS Sustain Chem Eng* 7:3267–3273. <https://doi.org/10.1021/acssuschemeng.8b05273>

- De Sá DS, da Rocha Rodrigues EJ, Suguihiro NM et al (2022) One-pot synthesis of carboxymethylcellulose-templated copper-NPs for heterocatalytic Huisgen-click reactions on lignocellulosic bamboo slices. *Catal Lett.* <https://doi.org/10.1007/s10562-022-03923-6>
- Gezici-Koç Ö, Erich SJF, Huinink HP et al (2017) Bound and free water distribution in wood during water uptake and drying as measured by 1D magnetic resonance imaging. *Cellulose* 24:535–553. <https://doi.org/10.1007/s10570-016-1173-x>
- Ginoble Pandoli O, Martins RS, De Toni KLG et al (2019) A regioselective coating onto microarray channels of bamboo with chitosan-based silver nanoparticles. *J Coat Technol Res* 16:999–1011. <https://doi.org/10.1007/s11998-018-00175-1>
- Ginoble Pandoli O, Paciornik S, Strauss M, Santhiago M (2022) Bamboo-based microfluidic system for sustainable bio-devices. *Bionics and sustainable design*. In: Palombini F (ed) *Bionics and sustainable design. Environmental footprints and eco-design of products and processes*. Springer, Singapore, pp 141–169. [https://doi.org/10.1007/978-981-19-1812-4\\_6](https://doi.org/10.1007/978-981-19-1812-4_6)
- Ginoble Pandoli O, Santos de Sá D, Nogueira Barbosa Junior M, Paciornik S (2023) Bamboo-based lignocellulose biomass as catalytic support for organic synthesis and water treatments. In: Palombini FL, Nogueira FM (eds) *Bamboo science and technology. Environmental footprints and eco-design of products and processes*. Springer, Singapore, pp 297–327. [https://doi.org/10.1007/978-981-99-0015-2\\_11](https://doi.org/10.1007/978-981-99-0015-2_11)
- Hao H, Tam L, Lu Y, Lau D (2018) An atomistic study on the mechanical behavior of bamboo cell wall constituents. *Compos Part B Eng* 151:222–231. <https://doi.org/10.1016/j.compositesb.2018.05.046>
- Jansen D, Naber C, Ectors D et al (2018) The early hydration of OPC investigated by in-situ XRD, heat flow calorimetry, pore water analysis and 1H NMR: learning about adsorbed ions from a complete mass balance approach. *Cem Concr Res* 109:230–242. <https://doi.org/10.1016/j.cemconres.2018.04.017>
- Ji Z, Ma J-F, Zhang Z-H et al (2013) Distribution of lignin and cellulose in compression wood tracheids of *Pinus yunnanensis* determined by fluorescence microscopy and confocal Raman microscopy. *Ind Crops Prod* 47:212–217. <https://doi.org/10.1016/j.indcrop.2013.03.006>
- Jin C, Li J, Han S et al (2015a) Silver mirror reaction as an approach to construct a durable, robust superhydrophobic surface of bamboo timber with high conductivity. *J Alloys Compd* 635:300–306. <https://doi.org/10.1016/j.jallcom.2015.02.047>
- Jin C, Yao Q, Li J et al (2015b) Fabrication, superhydrophobicity, and microwave absorbing properties of the magnetic  $\gamma$ -Fe<sub>2</sub>O<sub>3</sub>/bamboo composites. *Mater Des* 85:205–210. <https://doi.org/10.1016/j.matdes.2015.07.016>
- Kuan C, York RL, Cheng C (2015) Lignocellulose-based analytical devices: bamboo as an analytical platform for chemical detection. *Nat Publ Gr.* <https://doi.org/10.1038/srep18570>
- Li J, Ma E (2021) Characterization of water in wood by time-domain nuclear magnetic resonance spectroscopy (TD-NMR): a review. *Forests* 12:886. <https://doi.org/10.3390/f12070886>
- Li J, Ma E (2022) 2D time-domain nuclear magnetic resonance (2D TD-NMR) characterization of cell wall water of *Fagus sylvatica* and *Pinus taeda* L. *Cellulose* 29:8491–8508. <https://doi.org/10.1007/s10570-022-04789-y>
- Li J, Wu Z, Bao Y et al (2017a) Wet chemical synthesis of ZnO nanocoating on the surface of bamboo timber with improved mould-resistance. *J Saudi Chem Soc* 21:920–928. <https://doi.org/10.1016/j.jscs.2015.12.008>
- Li X, Wang X, Zhang M (2017b) An investigation of the drying rate of water in wood at different relative humidities studied by time domain nuclear magnetic resonance. *BioResources.* <https://doi.org/10.15376/biores.12.2.2991-3000>
- Li J, Ma R, Lu Y et al (2022) Bamboo-inspired design of a stable and high-efficiency catalytic capillary microreactor for nitroaromatics reduction. *Appl Catal B Environ* 310:121297. <https://doi.org/10.1016/j.apcatb.2022.121297>
- Liu Z, Meyers MA, Zhang Z, Ritchie RO (2017) Functional gradients and heterogeneities in biological materials: Design principles, functions, and bioinspired applications. *Prog Mater Sci* 88:467–498. <https://doi.org/10.1016/j.pmatsci.2017.04.013>
- Liu R, Zhang S, Semple K et al (2021) Precise microcasting revealing the connectivity of bamboo pore network. *Ind Crops Prod* 170:113787. <https://doi.org/10.1016/j.indcrop.2021.113787>
- Longo S, Egizi F, Stagno V et al (2023) A multi-parametric investigation on waterlogged wood using a magnetic resonance imaging clinical scanner. *Forests* 14:276. <https://doi.org/10.3390/f14020276>
- Machado AHL, Pandoli O, Miranda LSM, de Souza ROMA (2014) Microreactors: new opportunities in chemical synthesis. *Rev Virtual Quím.* <https://doi.org/10.5935/1984-6835.20140068>
- Menegazzo I, Mammi S, Sgarbossa P et al (2020) Time domain nuclear magnetic resonance (TD-NMR) to evaluate the effect of potato cell membrane electroporation. *Innov Food Sci Emerg Technol* 65:102456. <https://doi.org/10.1016/j.ifset.2020.102456>
- Menegazzo I, Mammi S, Sieni E et al (2021) Single-sided time domain-nuclear magnetic resonance to study the effect of cell membrane electroporation on the water mobility in vegetal tissues. *Biointerface Res Appl Chem* 11:14127–14141. <https://doi.org/10.33263/BRIAC116.1412714141>
- Meyer M, Buchmann C, Schaumann GE (2018) Determination of quantitative pore-size distribution of soils with <sup>1</sup>H NMR relaxometry. *Eur J Soil Sci* 69:393–406. <https://doi.org/10.1111/ejss.12548>
- Mikac U, Merela M, Oven P et al (2021) Mr study of water distribution in a beech (*Fagus sylvatica*) branch using relaxometry methods. *Molecules.* <https://doi.org/10.3390/molecules26144305>
- Mohebbi B, Claussen J, Blümich B (2019) Fast and robust quantification of liquid inside thin fibrous porous materials with single-sided NMR. *Magn Reson Imaging* 56:131–137. <https://doi.org/10.1016/j.mri.2018.09.022>
- Muhammad A, de V Azeredo RB (2014) <sup>1</sup>H NMR spectroscopy and low-field relaxometry for predicting viscosity and API gravity of Brazilian crude oils—a comparative study. *Fuel* 130:126–134. <https://doi.org/10.1016/j.fuel.2014.04.026>

- Nogata F, Takahashi H (1995) Intelligent functionally graded material: bamboo. *Compos Eng* 5:743–751. [https://doi.org/10.1016/0961-9526\(95\)00037-N](https://doi.org/10.1016/0961-9526(95)00037-N)
- Palma BG, Raquel RA, Rodrigo RO, Pandoli OG (2020) Immobilization of lipases on lignocellulosic bamboo powder for biocatalytic transformations in batch and continuous flow. *Catal Today*. <https://doi.org/10.1016/j.cattod.2020.04.041>
- Palombini FL, Nogueira FM, Kindlein W et al (2020) Biomimetic systems and design in the 3D characterization of the complex vascular system of bamboo node based on X-ray microtomography and finite element analysis. *J Mater Res* 35:842–854. <https://doi.org/10.1557/jmr.2019.117>
- Pandoli O, Martins RDS, Romani EC et al (2016) Colloidal silver nanoparticles: an effective nano-filler material to prevent fungal proliferation in bamboo. *RSC Adv* 6:98325–98336. <https://doi.org/10.1039/c6ra12516f>
- Pandoli OG, Neto RJG, Oliveira NR et al (2020) Ultra-highly conductive hollow channels guided by a bamboo biotemplate for electric and electrochemical devices. *J Mater Chem A* 8:4030–4039. <https://doi.org/10.1039/c9ta13069a>
- Peng Z, Zhang C, Zhang Y et al (2013) Transcriptome sequencing and analysis of the fast growing shoots of moso bamboo (*Phyllostachys edulis*). *PLoS ONE* 8:e78944. <https://doi.org/10.1371/journal.pone.0078944>
- Plastino A, Gonçalves EC, da Silva PN et al (2017) Combining classification and regression for improving permeability estimations from  $^1\text{H}$  NMR relaxation data. *J Appl Geophys* 146:95–102. <https://doi.org/10.1016/j.jappgeo.2017.09.003>
- Prestes RA, Colnago LA, Forato LA et al (2007) A rapid and automated low resolution NMR method to analyze oil quality in intact oilseeds. *Anal Chim Acta* 596:325–329. <https://doi.org/10.1016/j.aca.2007.06.022>
- Ratzsch K-F, Friedrich C, Wilhelm M (2017) Low-field rheo-NMR: a novel combination of NMR relaxometry with high end shear rheology. *J Rheol (n Y N y)* 61:905–917. <https://doi.org/10.1122/1.4991513>
- Reichardt C, Welton T (2010) Solvents and solvent effects in organic chemistry. Wiley-VCH Verlag GmbH & Co KGaA, Weinheim
- Rodrigues EJR, Sebastião PJO, Tavares MIB (2017)  $^1\text{H}$  time domain NMR real time monitoring of polyacrylamide hydrogels synthesis. *Polym Test* 60:396–404. <https://doi.org/10.1016/j.polymertesting.2017.04.028>
- Rudzuck T, Förster E, Nirschl H, Guthausen G (2019) Low-field NMR for quality control on oils. *Magn Reson Chem* 57:777–793. <https://doi.org/10.1002/mrc.4856>
- ThermoFisher Scientific (2018) Avizo 9 user's guide. Thermo Sci Avizo Softw 9 User's Guide 96–99
- Sheng C, Yang N, Yan Y et al (2020) Bamboo decorated with plasmonic nanoparticles for efficient solar steam generation. *Appl Therm Eng* 167:114712. <https://doi.org/10.1016/j.applthermaleng.2019.114712>
- Singer PM, Chen Z, Alemany LB et al (2018) Interpretation of NMR relaxation in bitumen and organic shale using polymer-heptane mixes. *Energy Fuels* 32:1534–1549. <https://doi.org/10.1021/acs.energyfuels.7b03603>
- Stagno V, Capuani S (2022) Decay of a Roman age pine wood studied by micro magnetic resonance imaging, diffusion nuclear magnetic resonance and portable nuclear magnetic resonance. *ACTA IMEKO* 11:10. [https://doi.org/10.21014/acta\\_imeko.v11i1.1079](https://doi.org/10.21014/acta_imeko.v11i1.1079)
- Stagno V, Mailhiet S, Capuani S et al (2021) Testing 1D and 2D single-sided NMR on Roman age waterlogged woods. *J Cult Herit* 50:95–105. <https://doi.org/10.1016/j.culher.2021.06.001>
- Stagno V, Ricci S, Longo S et al (2022) Discrimination between softwood and hardwood based on hemicellulose content obtained with portable nuclear magnetic resonance. *Cellulose* 29:7917–7934. <https://doi.org/10.1007/s10570-022-04728-x>
- Steele RM, Korb J-P, Ferrante G, Bubici S (2016) New applications and perspectives of fast field cycling NMR relaxometry. *Magn Reson Chem* 54:502–509. <https://doi.org/10.1002/mrc.4220>
- Valckenborg RME, Pel L, Hazrati K et al (2001) Pore water distribution in mortar during drying as determined by NMR. *Mater Struct* 34:599–604. <https://doi.org/10.1007/BF02482126>
- Wang J, Wang Y, Wu Y, Zhao W (2022) A multilayer transparent bamboo with good optical properties and UV shielding prepared by different lamination methods. *ACS Sustain Chem Eng* 10:6106–6116. <https://doi.org/10.1021/acssuschemeng.2c01719>
- Xu Y, Wong M, Yang J et al (2011) Dynamics of carbon accumulation during the fast growth period of bamboo plant. *Bot Rev* 77:287–295. <https://doi.org/10.1007/s12229-011-9070-3>
- Youssefian S, Rahbar N (2015) Molecular origin of strength and stiffness in bamboo fibrils. *Sci Rep* 5:11116. <https://doi.org/10.1038/srep11116>
- Zhang C, Li P, Zhang Y et al (2016) Hierarchical porous structures in cellulose: NMR relaxometry approach. *Polymer (guildf)* 98:237–243. <https://doi.org/10.1016/j.polymer.2016.06.036>

**Publisher's Note** Springer Nature remains neutral with regard to jurisdictional claims in published maps and institutional affiliations.